AFRL-AFOSR-VA-TR-2020-0156

Group IV Quantum Dots for Integrated Photonics

Matthew Panthani
IOWA STATE UNIVERSITY

07/21/2020
Final Report

Air Force Research Laboratory
AF Office Of Scientific Research (AFOSR)/ RTB1
Arlington, Virginia 22203
Air Force Materiel Command

DISTRIBUTION A: Distribution approved for public release.

REPORT DOCUMENTATION PAGE

Form Approved
OMB No. 0704-0188

1. REPORT DATE *(DD-MM-YYYY)*	2. REPORT TYPE	3. DATES COVERED *(From - To)*
01-09-2020	Final Performance	01 Mar 2017 to 29 Feb 2020

4. TITLE AND SUBTITLE
Group IV Quantum Dots for Integrated Photonics

5a. CONTRACT NUMBER

5b. GRANT NUMBER
FA9550-17-1-0170

5c. PROGRAM ELEMENT NUMBER
61102F

6. AUTHOR(S)
Matthew Panthani

5d. PROJECT NUMBER

5e. TASK NUMBER

5f. WORK UNIT NUMBER

7. PERFORMING ORGANIZATION NAME(S) AND ADDRESS(ES)
IOWA STATE UNIVERSITY
1350 BEARDSHEAR HALL
AMES, IA 50011 US

8. PERFORMING ORGANIZATION REPORT NUMBER

9. SPONSORING/MONITORING AGENCY NAME(S) AND ADDRESS(ES)
AF Office of Scientific Research
875 N. Randolph St. Room 3112
Arlington, VA 22203

10. SPONSOR/MONITOR'S ACRONYM(S)
AFRL/AFOSR RTB1

11. SPONSOR/MONITOR'S REPORT NUMBER(S)
AFRL-AFOSR-VA-TR-2020-0156

12. DISTRIBUTION/AVAILABILITY STATEMENT
A DISTRIBUTION UNLIMITED: PB Public Release

13. SUPPLEMENTARY NOTES

14. ABSTRACT
Silicon-based electronic computing is running into fundamental limitations related to on-chip communication. Another computing concept that can improve computing performance - as well as reduce their size, weight, and power consumption -is integrated photonics. However, integrated photonic circuits have been challenging to achieve due to the limitations of existing materials. Our team has developed new types of nanostructured Group IV (Si-Ge-Sn) alloys that could serve as onchip light emitters. We have probed their structural and optical properties using optical spectroscopy, NMR, and diffraction. We demonstrate their potential for integrated photonics by proof-of-concept optoelectronic devices.

15. SUBJECT TERMS
Integrated Photonics, Quantum Dots, Group IV, SiGeSn, material growth, silicon based photonics

16. SECURITY CLASSIFICATION OF:			17. LIMITATION OF ABSTRACT	18. NUMBER OF PAGES	19a. NAME OF RESPONSIBLE PERSON
a. REPORT	b. ABSTRACT	c. THIS PAGE			POMRENKE, GERNOT
Unclassified	Unclassified	Unclassified	UU		19b. TELEPHONE NUMBER *(Include area code)* 703-696-8426

Standard Form 298 (Rev. 8/98)
Prescribed by ANSI Std. Z39.18

Group IV Quantum Dots for Integrated Photonics

Grant Number: FA9550-17-1-0170

BAA-AFRL-AFOSR-2016-0006 (Air Force Office of Scientific Research Young Investigator Program)

Final Report. June 30, 2020

A. Investigators

Principal Investigator: Matthew G. Panthani, Assistant Professor of Chemical and Biological Engineering, Iowa State University

Other Personnel:

- Rainie Nelson, Graduate Student, Chemical Engineering, Iowa State University
- Yujie Wang, Graduate Student, Chemical Engineering, Iowa State University
- Bradley J. Ryan, Graduate Student, Chemical Engineering, Iowa State University
- Utkarsh Ramesh, Graduate Student, Chemical Engineering, Iowa State University

B. Abstract

Silicon-based electronic computing is running into fundamental limitations related to on-chip communication. Another computing concept that can improve computing performance - as well as reduce their size, weight, and power consumption - is integrated photonics. However, integrated photonic circuits have been challenging to achieve due to the limitations of existing materials. Our team has developed new types of nanostructured Group IV (Si-Ge-Sn) alloys that could serve as on-chip light emitters. We have probed their structural and optical properties using optical spectroscopy, NMR, and diffraction. We demonstrate their potential for integrated photonics by proof-of-concept optoelectronic devices.

C. Motivation and Background

Digital computing is currently based on microelectronic circuits that consist of logic units connected by of thin metal wires. Modern microprocessors have as much as *sixty miles* of wiring that is nanoscale in thickness.[1] As wire thicknesses have scaled down, resistive heating has become a problem that limits the processing speed of modern computer chips. This problem of heat generation caused clock speeds of processors to flatline around 2005,[2] after decades of exponential increases. While other computer engineering innovations have helped overcome the processing limitations in the short term, experts anticipate that improved clock speeds will become necessary to meet future needs. It is commonly accepted that *integrated photonics*, which replace the metal wiring with optical interconnects, is the most likely path forward.[3]

Optical data transfer is a well-established technology; *telecommunication technologies* are now primarily carried out through optical fibers worldwide. However, interfacing high-performance electronics with light-emitting materials on a single chip is technologically challenging. Currently,

commercially available integrated photonic circuits are created combining Si microelectronics with InP optical components using a bonding process. However, this strategy is not considered to be widely scalable because the processing of InP and other III-V semiconductors is *incompatible* with standard Complementary Metal-Oxide-Semiconductor (CMOS) manufacturing.[4] Thus, many do not anticipate that integrating III-V semiconductors onto Si will be able to provide the a solution that can be massively scaled up to create dense integrated photonic circuits in a cost-effective manner.[5] This points toward a need for *CMOS-compatible* optoelectronic materials.

Group IV-based optoelectronics. While Si, Ge, and their alloys are CMOS-compatible, they are also *indirect band gap* semiconductors and do not efficiently emit light upon optical or electronic excitation, as light emission is dipole-forbidden. However, their relevance to the existing microelectronics architecture has motivated alternative strategies for achieving light emission using Group IV semiconductors. For example, in the 1980's, Ennen and coworkers demonstrated that by doping Si with Er^{3+}, electroluminescence could be achieved at low temperatures (77K).[6] The luminescence was sharp, centered at 1.54 μm, arising from the 4f - 4f transition of Er^{3+}. Er-doped Si and SiO_2 have been used as a gain medium for optically-pumped lasers;[7] however, despite decades of research, there has been no reported electrically pumped rare-earth doped lasers on Si. Another interesting approach has been the Si Raman laser,[8] which relies on stimulated Raman scattering rather than stimulated electronic transitions. While this approach has achieved narrow linewidth in the mid-infrared and sparked new interest in Si photonics, Raman lasers inherently require external optical pumping and thus unlikely to become a feasible solution.

It has been proposed that *breaking symmetry* of Group IV semiconductors could open up pathways to achieving luminescenct Group IV semiconductors.[9] One recent approach has been to dope Si_XGe_{1-X} with Sn; Sn is much larger than Si or Ge and exhibit photoluminescence that has been attributed to *strain-induced lattice distortions*. The lattice distortions break diamond cubic symmetry, giving more direct-like character to the band structure. Electrically-pumped lasing has been demonstrated at wavelengths of ~2.0 μm and longer under cryogenic conditions for Si-Ge-Sn thin films.[10] These devices could have interesting applications in sensing applications, for example in "spectrometer-on-a-chip"-type devices. However, to be capable with today's telecommunication infrastructure, emission must occur at (or above) room temperature. Other approaches to achieving light emission in Group IV nanomaterials has been *size confinement*, such Canham's seminal work in porous Si,[11,12] or Si quantum dots that have size-dependent photoluminescence (**Fig 2**).[13]

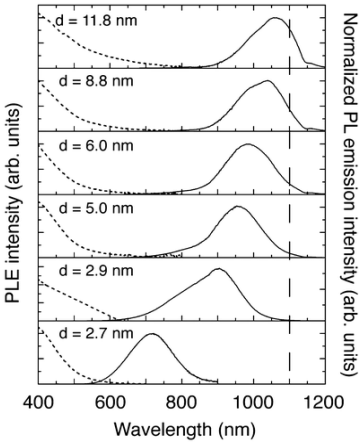

Figure 1. Room temperature photoluminescence emission (λ_{exc} = 420 nm) and excitation (measured at emission maximum) spectra of Si QDs (diameter 2.7 - 11.8 nm). The vertical dashed line indicates the position of the bulk Si band gap (1100 nm). [Hessel, Panthani, *Chem Mater*, 2011]. Reprinted with permission from the American Chemical Society. Copyright 2011.

Two-dimensional materials have unique optical and electronic properties that may be useful fornanosheets were synthesized in the early 1860's by Wöhler,[14] who deintercalated a layered $CaSi_2$ and obtained a yellow powder that is now believed to be monolayer Si. In the 1920's Kautsky called this material "siloxene,"[15] a name that was adopted for a time within the rest of the scientific community.[16,17] Over the years, there have been scattered reports of sheet-like materials comprised of Ge or Si with either hydrogen or hydroxyl termination.[16–21] However, the potential use of these materials for optoelectronic applications such as integrated photonics was not recognized until decades later.[22] Interest in Group IV analogues to graphene emerged in the past decade, with reports of "silicene"[23–27] and "germanene"[28,29] that are comprised of single monolayers of silicon and germanium, respectively. Unlike carbon, however, Si and Ge do not form stable sp^2-hybidized bonds; thus these samples were stable only in ultrahigh vacuum. In 2013, Goldberger characterized the stability of "germanane" a hydrogen-terminated germanium sheet that was synthesized from topochemical deintercalation of a layered $CaGe_2$.[30] Several more recent studies have expanded upon the surface chemistry of germanane and Sn-containing alloys.[31]

There are several promising features of 2D Group IV materials that encourage further study. Monolayer Si has been predicted to have exceptionally high charge carrier mobilities that are much higher than bulk Si ($\mu > 10^5$ $cm^2V^{-1}s^{-1}$).[32] Silicane and germanane both emit light,[33] despite the fact that the parent materials are indirect bandgap semiconductors. Unlike III-V semiconductors that are currently used for commercial integrated photonic circuits, these materials will not introduce elements that introduce deep traps into Si electronic components. This combination of potential for *excellent transport*, *strong and tunable photoluminescence* and *chemical compatibility* with CMOS-based processing make these an exciting class of future materials for integrated photonics.

D. Results

D1. Synthesis of Group IV Nanocrystals with Controlled Size and Composition

Ge NC synthesis. As a starting point, we aimed to understand discrepancies in literature regarding optical properties of Ge and Ge-Sn quantum dots. As a starting point, we used a well-defined stoichiometric mixture of GeI_2/GeI_4 as the germanium source, with oleylamine as the solvent and n-BuLi as the reducing agent. After dissolving the desired amounts of GeI_4 and/or GeI_2 in oleylamine, the required amount of n-BuLi dissolved in octadecene was added under flowing nitrogen at 200 °C and the reaction mixture was subsequently heated to 300 °C wherein it was held for an hour. Based on this procedure, 4 trials were performed. **Table 1** details the experimental conditions of these trials:

Sample	GeI_4:GeI_2	Ramp rate (°C/min)	NC size (nm)
1	50:50	15	3.5 nm
2	75:25	15	4 nm
3	100:0	15	3 nm
4	100:0	2	3 nm

Table 1. Experimental conditions for colloidal Ge NC synthesis

Even though the sizes of the NC samples were small, Ge has a very small effective mass and thus is expected to show a large increase in photoluminescence wavelength. Nonetheless, as shown in **Fig 3**, we notice that the photoluminescence (PL) spectra show *no trend* with size. This implies that a *surface species is responsible for the PL* of the Ge NCs.

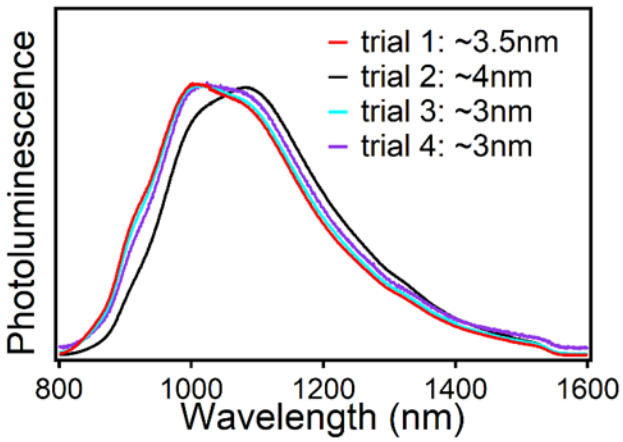

Figure 2. Photoluminescence spectra of different Ge NC samples with different sizes.

Ge_XSn_{1-X} NC synthesis. Here, we demonstrate the synthesis of Sn_xGe_{1-x} and report the findings from this procedure.

The synthesis uses a similar approach to the Ge NCs. Briefly, GeI_2 is added to oleylamine in a 3-necked flask at room temperature. The contents were degassed under vacuum to remove presence of oxygen and then backfilled with N_2. The tin source, $Sn(HMDS)_2$ was added to the flask, following which the flask was heated up to a target temperature. Once this temperature was achieved, n-BuLi in a cyclohexane solution was added to the flask as a reducing agent. The flask was then removed from the heating mantle, and the NC's were collected and dispersed in toluene.

Based on the above synthesis approach, 5 trials were performed. Each trial had a specific end size of the NC's which was taken from the supporting information of the original paper. **Table 2**

highlights the size (measured by transmission electron microscopy, shown in **Fig 3**) and composition (as measured by energy dispersive x-ray spectroscopy) of the different trials

Trial Number	NC size (nm)	Sn content (percent)
1	11.9	32
2	10.7	35
3	7.7	7.7
4	10.7	36
5	7.7	7.7

Table 2. Size and Sn content of various samples of Ge-Sn NCs.

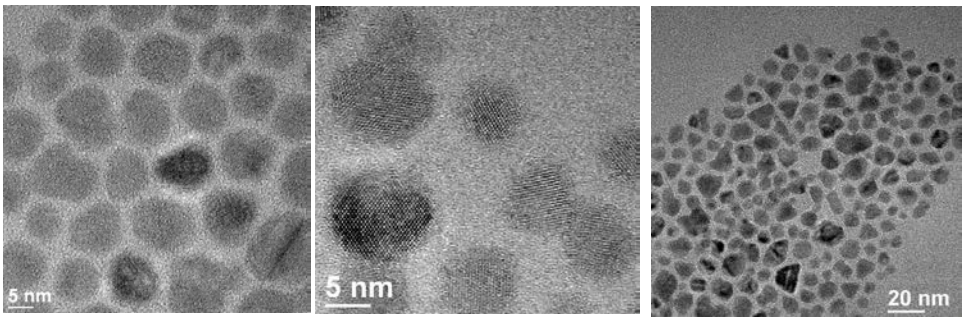

Figure 3. TEM images of Ge-Sn alloy NCs.

D.2. Solid-State Synthesis of Group IV Quantum Dots.

To test our hypothesis that the PL of colloidally-synthesized Ge-NCs originates from surface states, exploried solid state synthesis approaches that are expected to result in clean, hydrogen- or chlorine-terminated surfaces.[34] We synthesized GeO_X from a $GeCl_2$: dioxane complex. The GeO_X is an orange solid, and upon annealing at temperatures around 400°C it is converted to a black powder that consists of Ge NCs embedded in a GeO_2 matrix. The Ge NCs are etched with HF or HCl and collected. **Fig 4** shows TEM images of the Ge nanocrystals synthesized using this approach along with XRD confirming that they are crystalline Ge.

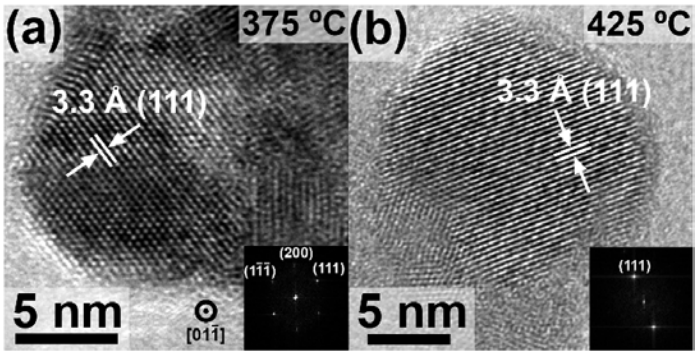

Figure 4. TEM images of nanocrystals obtained from hydrolyzed $GeCl_2$·dioxane annealed at (a) 375 °C and (b) 425 °C. The insets show the corresponding FFT pattern indexed to diamond cubic Ge (Wang, 2019). Reprinted with permission from Royal Society of Chemistry. Copyright 2019.

D.3. Synthesis and Characterization of Group IV Nanosheets.

We explored synthetic routes to monolayer Group IV nanomaterials using layered Zintl phases as solid-state templates. One example of this is monolayer Si nanosheets (Si-NSs). The Si-NSs were synthesized by deintercalating the Zintl phase $CaSi_2$ in aqueous HCl at ~−30 °C. Scanning electron microscopy (SEM) images of the Si-NSs (**Fig 5 c,d**) reveal a morphology that resembles loosely stacked sheets that are not atomically registered with each other, consistent with deintercalation of Ca^{2+}. This lack of registry prevents isolation of extended crystals of stacked Si-NSs, and is corroborated by the photograph in Figure 1a, which shows a large volume expansion accompanying deintercalation, indicating an increase in Si-NS interlayer separation. Transmission electron microscopy (TEM) images show the presence of stacks and few-layer wrinkled sheets (Figure 1e and Figure S1). The decrease in particle size after deintercalation likely arises from agitation provided by stirring during the deintercalation step

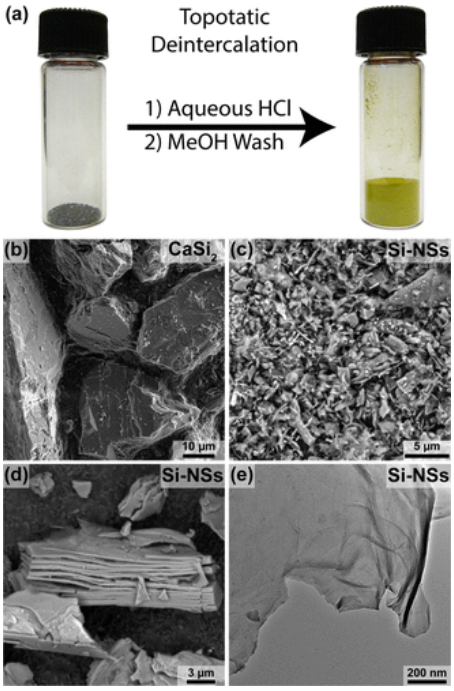

Figure 5. (a) Reaction schematic with images before and after deintercalation. The volume of powders is representative of the reaction. SEM images of (b) $CaSi_2$, (c) representative area of the Si-NSs, and (d) selected area of large Si-NSs. (e) TEM image of a few-layer-thick stack of Si-NSs. (Ryan, 2020) Reprinted with permission from American Chemical Society. Copyright 2020.

The surface chemistry of the SI-NSs was characterized using Raman spectroscopy, Fourier transform infrared spectroscopy (FTIR) and solid-state NMR. In the Raman spectrum (**Fig 6a**) the peak at 375 cm^{-1} is likely Si–Si vibrations, which also exist in $CaSi_2$ at 387 cm^{-1}; this was confirmed using a density functional theory simulation. The peaks at 375 and 489 cm^{-1} are red-shifted in comparison to $CaSi_2$, which is characteristic of phonon confinement effects that are expected to result from increased inter-sheet separation. The peak at 489 cm^{-1} agrees well with previous theoretical results of monolayer Si. The peaks at 511 and ~945 cm^{-1} are attributed to bulk-Si impurities. Weak SiOH features are observed between ~3300 and 3800 cm^{-1}, which likely arise from the Si-NSs and the Si-containing impurities.

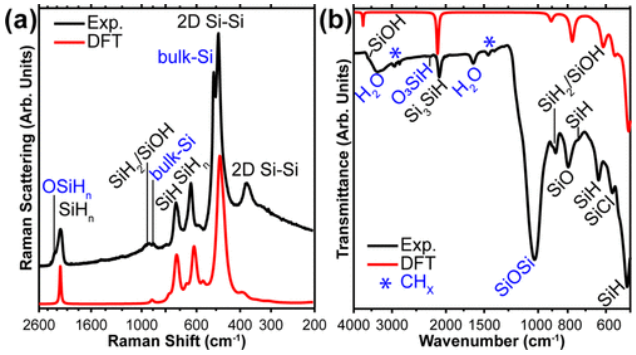

Figure 6. (a) Raman and (b) FTIR spectra of the Si-NSs. See Table S2 (Table S3) for complete Raman (FTIR) peak assignments. Peaks labeled in blue were intentionally not modeled with DFT. Note that the x axes are plotted on a logarithmic scale, increasing the apparent width of all peaks at low wavenumber while compressing the width of all peaks at high wavenumber. Black and red curves are experimental data and DFT simulations, respectively. (Ryan, 2020) Reprinted with permission from American Chemical Society. Copyright 2020.

High-resolution magic angle spinning (MAS) ^{1}H and ^{29}Si solid-state NMR spectroscopy were used to investigate the structure of the Si-NSs. The ^{1}H NMR signals at 3.9 and 6.0 ppm are assigned to Si_3SiH, while the signal at 1.3 ppm is likely Si_3SiOH (**Fig 7a**). A ^{1}H–^{1}H dipolar double quantum single quantum homonuclear correlation (DQ-SQ) spectrum demonstrates SiH_x species correlate to themselves and all other ^{1}H signals, indicating that all of these hydrogen sites are proximate within a Si-NS, consistent with the 2D ^{29}Si scalar DQ-SQ spectrum.

A 2D ^{29}Si–^{29}Si scalar DQ-SQ spectrum was obtained with the refocused INADEQUATE pulse sequence to determine whether the ^{29}Si signals at ±10 and −70 ppm arise from Si atoms within the NSs (**Fig 7c**). The DQ-SQ spectrum shows intense autocorrelation at −200 (−100) ppm in the DQ (SQ) dimensions, confirming Si–Si bonds between SiH groups within the sheets. The INADEQUATE spectrum also shows that signals at ±10 ppm arise from Si atoms that are directly bonded to SiH groups. The ^{29}Si signals at ±10 ppm are absent from 1D and 2D ^{1}H–^{29}Si INEPT spectra, suggesting that they lack SiH bonds. Thus, we conclude that the ^{29}Si signals at ±10 ppm likely correspond to Si_3SiX groups (where $X \neq H$). These signals could arise from Si_3SiCl or Si_3SiOH; however, no autocorrelations are observed for the Si_3SiX signals, suggesting that any SiX groups are isolated within the sheets and there are few XSi–SiX bonds. Chemical shifts were predicted with DFT on structural models similar to those used for the predictions of FTIR and Raman spectra. The calculated and experimental chemical shifts are in good agreement, confirming the NMR assignments.

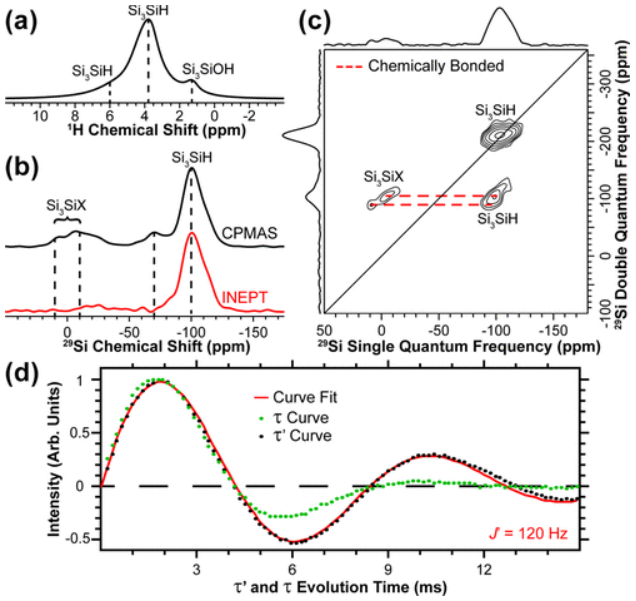

Figure 7. (a) MAS 1H solid-state NMR spectrum (vrot = 25 kHz). (b) Comparison of CPMAS (CP contact time of 6 ms) and 1H–29Si refocused INEPT (τ′ and τ mixing times of 1.44 ms). Dashed lines are shown to guide the eye. (c) Natural-abundance ^{29}Si–^{29}Si scalar DQ-SQ spectrum acquired with τ1/4J (MAS frequency) of 6 ms (10 kHz). Dashed red lines indicate chemically bonded 29Si spins. (d) INEPT τ and τ′ J-evolution curves with a fit of the τ′ curve to determine 1JSiH. (Ryan, 2020) Reprinted with permission from American Chemical Society. Copyright 2020.

A Kubelka–Munk (KM) transformation of diffuse reflectance demonstrates that the Si-NSs have optical features similar to those of previous reports (**Fig 8a**). Tauc analysis of the KM data indicates a direct band gap of 2.53 eV; DFT predicts an indirect band gap of 2.16 eV that is energetically close to a direct transition at 2.26 eV. DFT predictions of the extinction coefficient demonstrate a shoulder between ~2.3 and 3 eV—a feature not present in the experimental KM data—which is attributed to the conduction band with energies below ~3 eV (**Fig 8c**). The onset of ε is attributed to the direct transition $\Gamma_{V1} \rightarrow \Gamma_{C1}$. The sharp increase of ε at ~3.2 eV correlates to the increased density of states (DOS) at ~3.2–4.1 eV and the optically allowed transition $M_{V1} \rightarrow M_{C1}$ (transition of 3.6 eV). We therefore conclude that the experimental Si-NSs have a larger DOS at the absorption onset in comparison to the simulated models; we speculate that this increased DOS arises from defects. It has been reported that hydroxyl groups and chlorination can induce a direct transition within Si-NSs. We ascribe the KM peak at 3.2 eV to the electronic transition associated with the Si_6 framework, corresponding to the ε peak at ~4 eV, arising from the direct transition near M and the Si(p) → Si(p) transition from $\Gamma_{V1} \rightarrow \Gamma_{C2}$ (transition of 3.91 eV).

Photoluminescence (PL) spectra were collected from a dispersion of Si-NSs in methanol (**Fig 8b**). The PL maximum occurs near the absorption onset, which is characteristic of direct band gap behavior. The peak is centered at 500 nm (2.48 eV), closely matching the band gap estimated using Tauc analysis, assuming a direct band gap. The PL spectrum is asymmetric and has a full width at half-maximum (fwhm) of ~0.37 eV. By fitting the PL to two Gaussian–Lorentz product distributions, we deconvoluted the spectrum into two distributions: a higher energy peak centered at 498 nm with a fwhm of 0.31 eV, comprising 64% of the total curve, and a lower energy peak centered at 543.9 nm with a fwhm of 0.48 eV, comprising 36% of the total curve. Time-resolved PL (TRPL) suggests a biexponential decay, with a shorter lifetime of ~4.1

ns and a longer lifetime of 110 ns; such short lifetimes provide additional evidence of direct band gap emission.

We estimate the PL quantum yield (PLQY) of a dispersion of the Si-NSs in methanol to be ~9%; however, the preparation of nonscattering dispersions limits our ability to accurately determine this value. This agrees well with a previous study that also determined a PLQY of 9%.Further experimental investigations on the influence of terminal SiOH and SiCl groups are needed to gain a better understanding of the origin of emission.

Fig 8c shows the band structure and projected density of states (pDOS) of silicane. The color of each band enables visualization of the hybridization of each band at a given wave vector. The Si(p) orbitals (blue line in the pDOS) contain the p_x, p_y, and p_z orbitals. It is observed that the H contribution to the band structure (red in the pDOS) includes bands at ca. −2.5 and 4 eV. Sharing of electrons between the H(s) and Si(p) orbitals results in hybridization in the DOS, as indicated by the purple lines in the band structure. We find that H is bound to Si through the Si(p_z) orbitals.

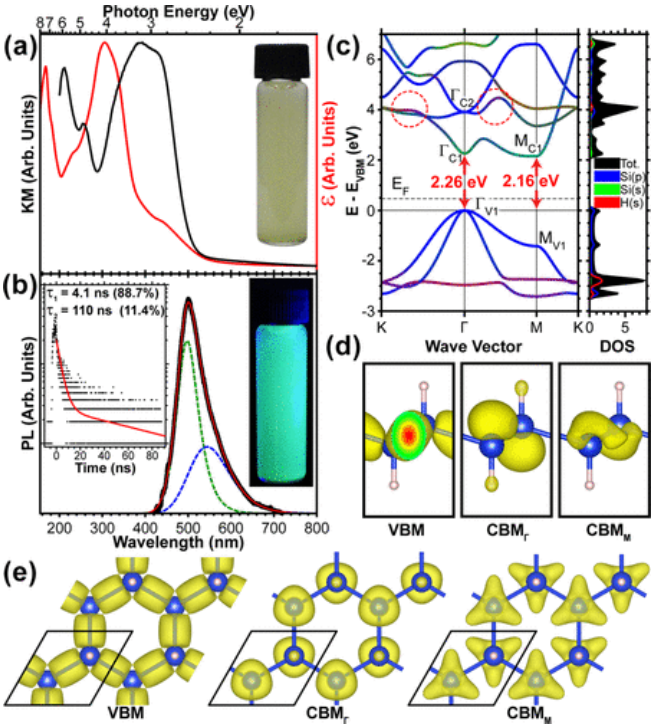

Figure 8. (a) Kubelka-Munk absorption (black) and simulated extinction coefficient (red). (b) Photoluminescence and its deconvolution. The excitation wavelength is 375 nm, the photo inset is of the dispersed sample under UV illumination, and the graph inset is TRPL. (c) Band structure and projected density of states (pDOS). The real-space orbitals at the valence band maximum (VBM) and conduction band minimum at Γ and M ($CBM_Γ$, CBM_M, respectively) viewed down the *a* and *c* axes are shown in (d) and (e), respectively. The unit cell is shown in black, and electron density isosurfaces are plotted at 0.0844 $Å^{-3}$. The red circles in (c) indicate the contribution of hydrogen, which is hypothesized to decrease the energy of the $CBM_Γ$. (Ryan, 2020) Reprinted with permission from American Chemical Society. Copyright 2020.

D.4. Electronic and Optoelectronic Devices

We synthesized methyl-terminated germanane flakes by modifying a procedure reported by Jiang *et al.*,[35] for details. The obtained flakes have large lateral dimensions reaching several microns, as revealed by microscopy images (**Fig 9a**). These germanane flakes are composed of stacks of individual layers (20–50 nm in thickness typically) of methyl-terminated germanane, as

revealed by TEM. Fourier-transform infrared (FTIR, **Fig 9d**) spectroscopy confirms the presence of methyl termination, with vibrational modes arising from C-H and Ge-C bonds, see. The Raman spectrum reveals a main contribution appearing at 299 cm^{-1} which is associated with the E_{2g} mode. A second contribution arising from the methyl functionalization appears at 594 cm^{-1}. The X-ray diffraction, in particular, reveals a peak around $2\theta \approx 7.9°$, which, along with Raman and Fourier transform infrared spectroscopy, confirms that the sample contains Ge sheets that are terminated with $-CH_3$ groups. From Bragg's law, the periodicity of the material is found to be ≈1.1 nm, corresponding to an interplanar distance of 0.55 nm.

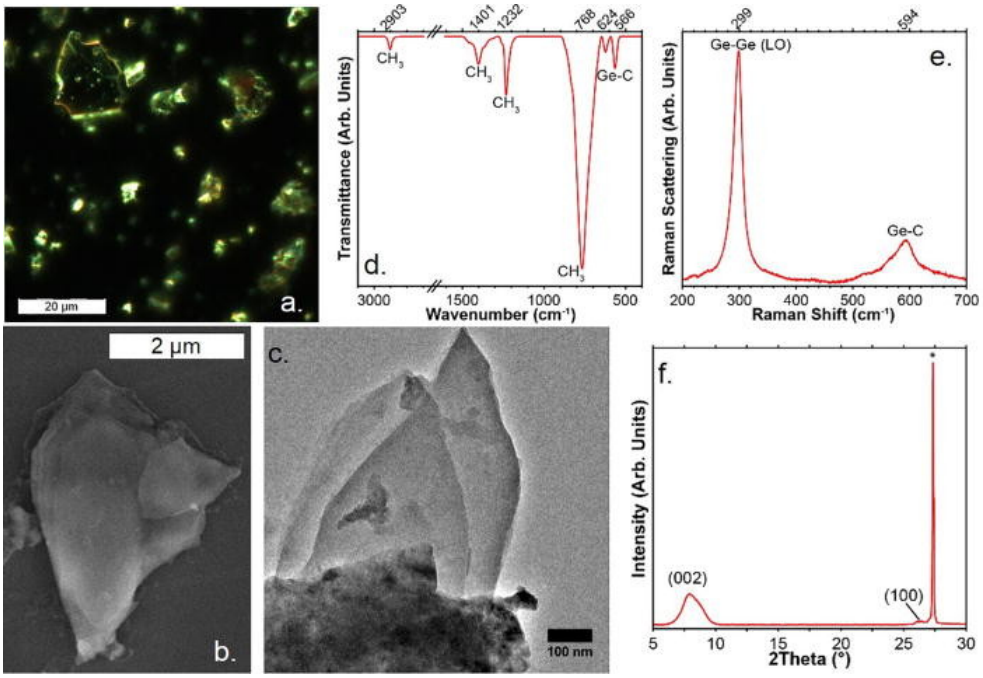

Figure 9. Dark-field optical (a), scanning electron (b), and transmission electron (c) microscopy images of the methyl-terminated germanane flakes. FTIR (d) and Raman (e) spectra of methyl-terminated germanane powder. (d) Powder X-ray diffraction pattern of methyl-terminated germanane; the narrow peak highlighted with an "asterisk" corresponds to bulk Ge. Reprinted with permission from American Institute of Physics Publishing. Copyright 2019.

To assess the electronic transport properties of germanane flake arrays, we constructed interdigitated electrodes using a conventional optical lithography method and drop-cast a dispersion of germanane flakes onto the electrodes. **Fig 10b** shows I-V characteristics of the germanane flake array at different temperatures. The arrays appear to be conductive, displaying decreasing conductance with decreasing temperature. Fitting the current-temperature curve to an Arrhenius law (**Fig 10a**) allows for the extraction of an activation energy of 118 meV in the vicinity of room temperature. Because this activation energy is much smaller than one half of the bandgap—the expected value for intrinsic semiconductors—this suggests residual doping within the material. To determine the nature of this doping, we integrated the material in a field effect transistor. We use an ion gel electrolyte gating which has proven to be a viable approach for low gate bias field effect transistors made from colloidal nanocrystals and other types of 2D materials, as shown in the schematic in **Fig 10c**. The transfer curve (**Fig 10d**) reveals p-type

character for the methyl-terminated germanane flake arrays; this is consistent with previous observations obtained using a back gated geometry. The on/off ratio of the transistor reached a factor of 250 over only ±2 V of gate bias operation. It is also worth pointing that the turn-on voltage of the transistor is around 100 mV, which is very similar to the activation energy determined from the I-T curve. This suggests that the Fermi level of the material lies in the vicinity (100 ± 20 meV) of the valence band.

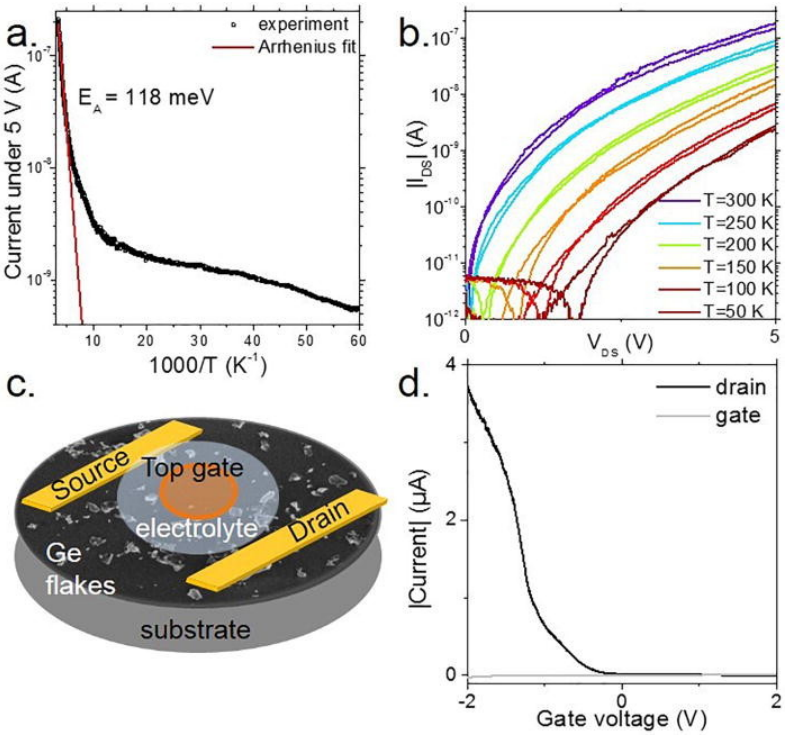

Figure 10. (a) Diagram of an electrolyte gated field effect transistorwith a channel made from methyl-terminated germanane. (b) IV characteristics of methyl-terminated germanane flakes at various temperatures. (c) Current as a function of temperature for a thin film of methyl-terminated germanane at various temperatures. (d) Drain and gate current as a function of the applied gate bias for an electrolyte gated methyl-terminated germanane-based field effect transistor. Reprinted with permission from American Institute of Physics Publishing. Copyright 2019.

Under illumination, arrays of methyl-terminated germanane flakes display a positive photoresponse (i.e., a rise in conductance under illumination), as shown in **Fig 11a**. The rise time response of the device is typically below 100 μs with a weak temperature dependence. This corresponds in the frequency domain to a 3 dB cut-off frequency above 1 kHz, **Fig 11b**. The power dependence of the photoresponse appears to present a power law dependency where the exponent is close to 0.5, as shown in **Fig 11c**. This suggests that the photocarrier lifetimes are limited by band-to-band recombination rather than by trapping. This observation is consistent with the absence of traps in the PL spectrum at room temperature.

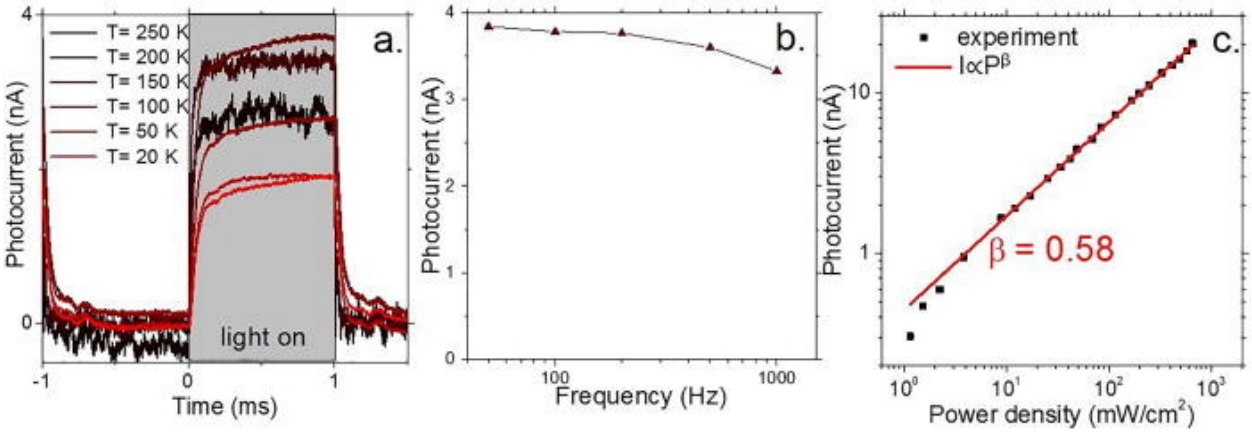

Figure 11. (a) Transient photocurrent measurements of germanane phototransistors ($\lambda = 405$ nm; $P \approx 2$ mW), at different temperatures. The measurement is made under a +5 V bias. (b) Frequency dependence of the photocurrent (at room temperature). (c) Current as a function of light incident power. Reprinted from American Institute of Physics Publishing. Copyright 2019.

E. Conclusions and Future Work

The results from this grant have resulted in the development of new nanoscale light emitters comprised of Group IV elements (Si and Ge) that may be used as components for integrated photonic circuits. They can be synthesized at large scales, and the 2D materials explored here have excellent light emitting properties. We have demonstrated their potential use for optoelectronic devices by fabricating proof-of-concept photodetector devices. Future research directions of interest to DoD will involve increasing Sn content in Group IV nanomaterials in effort to achieve efficient near-infrared emission and studying their photophysical behavior using ultrafast spectroscopy. This will invite opportunities to study other phenomena, such as lasing, in this new class of nanomaterials.

F. Publications resulting from funding

Peer-reviewed Publications

1. Ryan, B.J., Hanrahan, M.P., Wang, Y., Ramesh, U., Nyamekye, C.K., Nelson, R.D., Liu, Z., Huang, C., Whitehead, B., Wang, J. and Roling, L.T., (2019). Silicene, Siloxene, or Silicane? Revealing the Structure and Optical Properties of Silicon Nanosheets Derived from Calcium Disilicide. (2019) *Chemistry of Materials*, *in press.*

2. Wang, Y., Ramesh, U., Nyamekye, C.K., Ryan, B.J., Nelson, R.D., Alebri, A.M., Hamdeh, U.H., Hadi, A., Smith, E.A. Panthani, M.G., (2019). Synthesis of germanium nanocrystals from solid-state disproportionation of a chloride-derived germania glass. *Chemical Communications*, *55*(43), pp.6102-6105.

3. Hadi, A., Ryan, B.J., Nelson, R.D., Santra, K., Lin, F.Y., Cochran, E.W., Panthani, M.G., (2019). Improving the Stability and Monodispersity of Layered Cesium Lead Iodide

Perovskite Thin Films by Tuning Crystallization Dynamics. *Chemistry of Materials*. 31(14), 4990-4998

4. Hamdeh, U.H., Ryan, B.J., Nelson, R.D., Zembrzuski, M., Slobidsky, J., Prince, K.J., Cleveland, I., Vela-Ramirez, A., Hillier, A.C. and Panthani, M.G., (2019). Solution-Processed Bismuth Halide Perovskite Thin Films: Influence of Deposition Conditions and A-Site Alloying on Morphology and Optical Properties. *Journal of Physical Chemistry Letters*, 10(11), 3134-3139.

5. Hamdeh, U.H., Nelson, R.D., Ryan, B.J. and Panthani, M.G. (2019). The Effects of Solvent Coordination Strength on the Morphology of Solution-Processed BiI_3 Thin Films. *The Journal of Physical Chemistry C*. 123(22), 13394-13400

6. Livache, C., Ryan, B.J., Ramesh, U., Steinmetz, V., Gréboval, C., Chu, A., Brulé, T., Ithurria, S., Prévot, G., Barisien, T. and Ouerghi, A., Panthani, M.G., Lhuillier, E.. (2019) Optoelectronic properties of methyl-terminated germanane. *Applied Physics Letters*, *115*(5), 052106.

G. Presentations resulting from funding

Invited Presentations acknowledging AFOSR

1. Panthani, M.G., "Group IV Semiconductor Nanocrystals and Nanosheets: a Potential Route to Silicon-based Photonics", University of Florida Materials in Chemical Engineering Mini-Symposium, November 2019.

2. Panthani, M.G., "Optical and Optolectronic Properties of Nanoscale Group IV Semiconductors," 2nd AFRL Workshop on GeSn and GeSiSn. Dayton, OH. September 2019.

3. Panthani, M.G., "Colloidal Pb-free Halide Perovskite and Group IV Nanomaterials," ACS Fall 2019 National Meeting. San Diego, CA. August 2019.

4. Panthani, M.G., "Synthesis and Optical Properties of Colloidal Group IV Nanocrystals and Nanoplatelets," 2018 MRS Spring Meeting. Phoenix, AZ. Apr 25, 2019.

5. Panthani, M.G., "Quasi-two-dimensional Materials: Synthetic Challenges and Structure-tunable Properties," Ames Laboratory Seminar. Ames, IA. March 19, 2019.

6. Panthani, M.G., "Quasi-Two-Dimensional Materials: Synthetic Challenges and Structure-Tunable Properties," 2018 AIChE Annual Meeting. Pittsburgh, PA. Oct 31, 2018.

7. Panthani, M.G., "Crystallizing Semiconductors at the Nano- and Molecular Scale: Opportunities and Challenges," Case Western Reserve University, Department of Chemical and Biomolecular Engineering Seminar Series. Cleveland, OH. Oct 11, 2018.

8. Panthani, M.G., “Crystallizing Semiconductors at the Nano- and Molecular Scale: Opportunities and Challenges,” Colorado School of Mines, Chemical and Biological Engineering Seminar Series. Golden, CO. Oct 5, 2018

9. Panthani, M.G., “Crystallizing Semiconductors at the Nano- and Molecular Scale: Opportunities and Challenges,” National Renewable Energy Laboratory, Chemical and Material Sciences Seminar. Golden, CO. Oct 4, 2018

10. Panthani, M.G., “Crystallizing Semiconductors at the Nano- and Molecular Scale: Opportunities and Challenges,” Vanderbilt University, Vanderbilt Institute of Nanoscience and Engineering (VINSE) Seminar Series. Nashville, TN. Sep 12, 2018

11. Panthani, M.G., “Group IV Quantum Dots for Integrated Photonics,” AFOSR/AFRL SiGeSn Alloy and Related Materials Program Review. Dayton, OH. Jan 11, 2018.

12. Panthani, M.G., “Group IV Quantum Dots for Integrated Photonics,” 2017 Air Force Office of Scientific Research Young Investigator Meeting. Arlington, VA. Nov. 16, 2017.

Contributed Presentations acknowledging AFOSR

[1] Panthani, M.G., “Structural and Optical Properties of Deintercalated $CaGe_{2-2x}Si_{2x}$” North American Solid State Chemistry Conference. Golden, CO. July 2019.

[2] Panthani, M.G. “Synthesis and Optical Properties of Colloidal Group IV Nanocrystals and Nanoplatelets”. 2018 Materials Research Society Spring Meeting. Phoenix, AZ. April 2018.

H. References Cited

(1) Home-Douglas, P. LIGHT CIRCUITS. *ASEE Prism* **2015**, *24* (7), 12.
(2) Council, N. R. *The Future of Computing Performance: Game Over or Next Level?*; National Academies Press, 2011.
(3) Wilson, L. International Technology Roadmap for Semiconductors (ITRS). *Semicond. Ind. Assoc.* **2013**.
(4) Thomson, D.; Zilkie, A.; Bowers, J. E.; Komljenovic, T.; Reed, G. T.; Vivien, L.; Marris-Morini, D.; Cassan, E.; Virot, L.; Fédéli, J.-M. Roadmap on Silicon Photonics. *J. Opt.* **2016**, *18* (7), 073003.
(5) Zhou, Z.; Yin, B.; Michel, J. On-Chip Light Sources for Silicon Photonics. *Light Sci. Appl.* **2015**, *4* (11), e358. https://doi.org/10.1038/lsa.2015.131.
(6) Ennen, H.; Schneider, J.; Pomrenke, G.; Axmann, A. 1.54-μm Luminescence of Erbium-implanted III-V Semiconductors and Silicon. *Appl. Phys. Lett.* **1983**, *43* (10), 943–945.
(7) Pavlov, S. G.; Zhukavin, R. K.; Orlova, E. E.; Shastin, V. N.; Kirsanov, A. V.; Hübers, H.-W.; Auen, K.; Riemann, H. Stimulated Emission from Donor Transitions in Silicon. *Phys. Rev. Lett.* **2000**, *84* (22), 5220.

(8) Rong, H.; Liu, A.; Jones, R.; Cohen, O.; Hak, D.; Nicolaescu, R.; Fang, A.; Paniccia, M. An All-Silicon Raman Laser. *Nature* **2005**, *433* (7023), 292.
(9) Jalali, B.; Fathpour, S. Silicon Photonics. *J. Light. Technol.* **2006**, *24* (12), 4600–4615.
(10) Sun, G.; Soref, R. A.; Cheng, H. H. Design of an Electrically Pumped SiGeSn/GeSn/SiGeSn Double-Heterostructure Midinfrared Laser. *J. Appl. Phys.* **2010**, *108* (3), 033107.
(11) Canham, L. T. Silicon Quantum Wire Array Fabrication by Electrochemical and Chemical Dissolution of Wafers. *Appl. Phys. Lett.* **1990**, *57* (10), 1046–1048.
(12) Cullis, A. G.; Canham, L. T. Visible Light Emission Due to Quantum Size Effects in Highly Porous Crystalline Silicon. *Nature* **1991**, *353* (6342), 335.
(13) Hessel, C. M.; Reid, D.; Panthani, M. G.; Rasch, M. R.; Goodfellow, B. W.; Wei, J.; Fujii, H.; Akhavan, V.; Korgel, B. A. Synthesis of Ligand-Stabilized Silicon Nanocrystals with Size-Dependent Photoluminescence Spanning Visible to near-Infrared Wavelengths. *Chem. Mater.* **2011**, *24* (2), 393–401.
(14) Wohler, F. On the Reaction of Silicon with Oxygen and Hydrogen (Compunds). *Lieb Ann* **1863**, *127*, 264–274.
(15) Kautsky, H.; Thiele, H. Umsetzungen Des Siloxens Mit Halogenverbindungen Und Ihre Auslösung Durch Licht Und Chemische Reaktionen. *Z. Für Anorg. Allg. Chem.* **1925**, *144* (1), 197–217.
(16) Hengge, E. Color and Fluorescence of Cyclic Si Compounds II. Fluorescence and Color of Siloxene and Its Derivatives. *Chem Ber* **1962**, *95*, 648–657.
(17) Hengge, E. Siloxene and Sheetlike Silicon Subcompounds. *Fortschr Chem Forsch* **1967**, *9*, 145–164.
(18) Vogg, G.; Brandt, M. S.; Stutzmann, M. Polygermyne—a Prototype System for Layered Germanium Polymers. *Adv. Mater.* **2000**, *12* (17), 1278–1281.
(19) Hirabayashi, I.; Morigaki, K.; Yamanaka, S. Optical Properties of Disordered Silicide Layer Compound: Siloxene (Si6 (OH) 3H3)—Time Resolved Luminescence. *J. Non-Cryst. Solids* **1983**, *59*, 645–648.
(20) Seifert, G.; Köhler, T.; Hajnal, Z.; Frauenheim, T. Tubular Structures of Germanium. *Solid State Commun.* **2001**, *119* (12), 653–657.
(21) Hajnal, Z.; Vogg, G.; Meyer, L. J.-P.; Szűcs, B.; Brandt, M. S.; Frauenheim, T. Band Structure and Optical Properties of Germanium Sheet Polymers. *Phys. Rev. B* **2001**, *64* (3), 033311.
(22) Brus, L. Luminescence of Silicon Materials: Chains, Sheets, Nanocrystals, Nanowires, Microcrystals, and Porous Silicon. *J. Phys. Chem.* **1994**, *98* (14), 3575–3581.
(23) Aufray, B.; Kara, A.; Vizzini, S.; Oughaddou, H.; Leandri, C.; Ealet, B.; Le Lay, G. Graphene-like Silicon Nanoribbons on Ag (110): A Possible Formation of Silicene. *Appl. Phys. Lett.* **2010**, *96* (18), 183102.
(24) Fleurence, A.; Friedlein, R.; Ozaki, T.; Kawai, H.; Wang, Y.; Yamada-Takamura, Y. Experimental Evidence for Epitaxial Silicene on Diboride Thin Films. *Phys. Rev. Lett.* **2012**, *108* (24), 245501.
(25) Lalmi, B.; Oughaddou, H.; Enriquez, H.; Kara, A.; Vizzini, S.; Ealet, B.; Aufray, B. Epitaxial Growth of a Silicene Sheet. *Appl. Phys. Lett.* **2010**, *97* (22), 223109.
(26) Tao, L.; Cinquanta, E.; Chiappe, D.; Grazianetti, C.; Fanciulli, M.; Dubey, M.; Molle, A.; Akinwande, D. Silicene Field-Effect Transistors Operating at Room Temperature. *Nat. Nanotechnol.* **2015**, *10* (3), 227.

(27) Vogt, P.; De Padova, P.; Quaresima, C.; Avila, J.; Frantzeskakis, E.; Asensio, M. C.; Resta, A.; Ealet, B.; Le Lay, G. Silicene: Compelling Experimental Evidence for Graphenelike Two-Dimensional Silicon. *Phys. Rev. Lett.* **2012**, *108* (15), 155501.
(28) Dávila, M. E.; Xian, L.; Cahangirov, S.; Rubio, A.; Le Lay, G. Germanene: A Novel Two-Dimensional Germanium Allotrope Akin to Graphene and Silicene. *New J. Phys.* **2014**, *16* (9), 095002.
(29) Li, L.; Lu, S.; Pan, J.; Qin, Z.; Wang, Y.; Wang, Y.; Cao, G.; Du, S.; Gao, H.-J. Buckled Germanene Formation on Pt (111). *Adv. Mater.* **2014**, *26* (28), 4820–4824.
(30) Bianco, E.; Butler, S.; Jiang, S.; Restrepo, O. D.; Windl, W.; Goldberger, J. E. Stability and Exfoliation of Germanane: A Germanium Graphane Analogue. *ACS Nano* **2013**, *7* (5), 4414–4421. https://doi.org/10.1021/nn4009406.
(31) Arguilla, M. Q.; Jiang, S.; Chitara, B.; Goldberger, J. E. Synthesis and Stability of Two-Dimensional Ge/Sn Graphane Alloys. *Chem. Mater.* **2014**, *26* (24), 6941–6946. https://doi.org/10.1021/cm502755q.
(32) Shao, Z.-G.; Ye, X.-S.; Yang, L.; Wang, C.-L. First-Principles Calculation of Intrinsic Carrier Mobility of Silicene. *J. Appl. Phys.* **2013**, *114* (9), 093712.
(33) Stutzmann, M.; Brandt, M. S.; Rosenbauer, M.; Fuchs, H. D.; Finkbeiner, S.; Weber, J.; Deak, P. Luminescence and Optical Properties of Siloxene. *J. Lumin.* **1993**, *57* (1–6), 321–330.
(34) Wang, Y.; Ramesh, U.; Nyamekye, C. K.; Ryan, B. J.; Nelson, R. D.; Alebri, A. M.; Hamdeh, U. H.; Hadi, A.; Smith, E. A.; Panthani, M. G. Synthesis of Germanium Nanocrystals from Solid-State Disproportionation of a Chloride-Derived Germania Glass. *Chem. Commun.* **2019**, *55* (43), 6102–6105.
(35) Jiang, S.; Butler, S.; Bianco, E.; Restrepo, O. D.; Windl, W.; Goldberger, J. E. Improving the Stability and Optical Properties of Germanane via One-Step Covalent Methyl-Termination. *Nat. Commun.* **2014**, *5*, 3389. https://doi.org/10.1038/ncomms4389.